



# Engineered PMMA-ZnO nanocomposites for improving the electric arc interruption capability in electrical switching applications: Unprecedented experimental insights



Venkatesh Doddapaneni <sup>a, \*\*</sup>, Mohsin Saleemi <sup>a</sup>, Fei Ye <sup>a</sup>, Rudolf Gati <sup>b</sup>,  
Muhammet S. Toprak <sup>a, c, \*</sup>

<sup>a</sup> Department of Materials and Nano Physics, KTH Royal Institute of Technology, Isaffjordsgatan 22, SE 164 40 Kista, Sweden

<sup>b</sup> ABB Switzerland, Corporate Research, Segelhofstrasse 1K, 5405 Baden-Dättwil, Switzerland

<sup>c</sup> Department of Applied Physics, KTH Royal Institute of Technology, Albanova, Roslagstullsbacken 21, SE106 91 Stockholm, Sweden

## ARTICLE INFO

### Article history:

Received 18 October 2016

Received in revised form

26 November 2016

Accepted 6 January 2017

Available online 23 January 2017

### Keywords:

Polymer-matrix composites

Nano particles

Electrical arcs

Ablation

Arc interruption capability

## ABSTRACT

Polymer inorganic nanocomposites (PINCs) have been engineered for controlling the electrical arc and to improve the arc interruption capability of the electrical switching applications, like circuit breakers. Several PINCs are fabricated by formation of ZnO quantum dots (QDs) in a poly (methyl methacrylate) (PMMA) matrix via *in-situ* polymerization method to avoid agglomeration of QDs, leading to a good spatial distribution of QDs in the polymer matrix. These PINCs have been characterized in detail for the morphology of QDs, interaction between QDs and polymer matrix, and ultraviolet (UV) radiation absorption. ZnO QDs have been assessed to have particle diameter of 3.5 nm, and their presence in the PMMA is revealed by the unique luminescence characteristics of the QDs under UV light. The presence of ZnO QDs broadened the range of UV radiation absorption of PMMA and the absorption edge is gradually shifted from 270 nm to 338 nm with step-wise loading of ZnO QDs. The PINCs are tested to determine their reproducibility and impact on the electrical arcs of current 1.6 kA generated using a specially designed test-setup. Interaction of PINCs with the electrical arcs generates ablation of chemical species towards core of the electrical arc, resulting in increase of voltage leading to cool-down the arc temperature. This experimental study demonstrates for the first time that these PINCs are reproducible, reliable and provides superior arc interruption capability.

© 2017 Elsevier Ltd. All rights reserved.

## 1. Introduction

According to the present global power demand and supply, taking advantage of sustainable and reliable power sources, such as hydro, solar, sustainable heat and wind power, is the most urgent challenge that mankind is facing today [1–4]. In furtherance with United Nations climate change policy, low-carbon power generation share is expected to grow to almost 45% in 2030 by keeping current power emission flat, while electricity demand is expected to grow by more than 40% [2]. Under these circumstances, the present electricity grid has to be improved with better and efficient

technologies. One of the key technological components under this domain is the circuit breaker, which has been playing a key role at power generation, transmission and distribution levels since 1920's and their role is to safeguard the electrical grid from the faults by automatic interruption [5,6].

The circuit breaker is an automatic mechanical switching device, capable of controlling currents under the typical conditions, e.g., short-circuit and over currents. When it opens, it can generate an electrical arc, which has extreme conditions inside the breaker reaching temperature of 20,000 °C and pressure nearly 10–70 bar [5–7]. In order to protect from such conditions, ceramic plates have been widely used due to their high thermal protection capability. Since last decade, polymers have been used to cool down the arcs effectively in addition to the thermal protection and to avoid further damages to the breaker case and the electric grid [8,9]. When the intense radiative and thermal energy emitted by the arc impinges on the polymer surface as shown in illustrated

\* Corresponding author. Department of Applied Physics, KTH Royal Institute of Technology, Albanova, Roslagstullsbacken 21, SE106 91 Stockholm, Sweden.

\*\* Corresponding author.

E-mail addresses: [vdo@kth.se](mailto:vdo@kth.se) (V. Doddapaneni), [toprak@kth.se](mailto:toprak@kth.se) (M.S. Toprak).

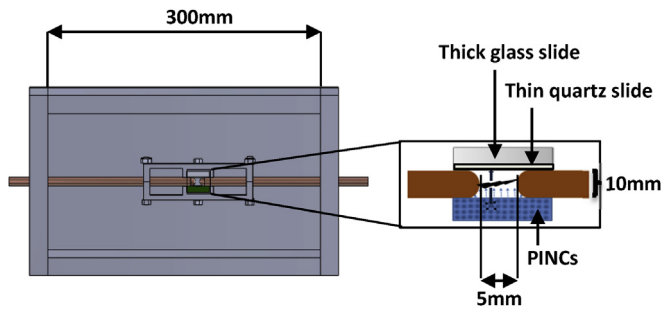


Fig. 1. Sketch of the designed electrical arc test-setup with schematic illustration of the radiative energy transfer between the electrical arc and PINCs.

Fig. 1, polymer ablates the chemical species, which are injected radially towards the arc. These species are divided mainly into two parts; one part enters into the arc region and heated to plasma temperature by absorption of radiation coming from the arc, while the other part is exhausted radially [10,11]. This process of controlling the electrical arcs by using the polymers is called as ablation-controlled electrical arcs [12–14]. Under these conditions, radiative energy transfer is the dominant energy transfer mechanism between the electrical arcs and polymer and 65% of radiated energy from the electrical arcs is mostly in UV region, verified experimentally and theoretically [12,15,16]. Therefore, enhancement on absorption of the intensive radiation from the electrical arcs is the driving force for development of new materials for circuit breaker.

Since the last decade, developments in the material science are augmented tremendously and recent research demonstrated that polymer inorganic nanocomposites (PINCs) can be rather promising candidates for improving the protection and reliability of the circuit breakers, by improving the control over the extreme conditions mentioned above. Tanaka et al. and Li et al. [14,17–23], opened up a new discussion on developing PINCs by using different nanoparticles for electrical switching, bio and optical applications [24–29]. However, these PINCs are not verified experimentally for protection from the high energy electrical arcs of current ranges ~1.6 kA generated in low voltage circuit breakers, due to the experimental complexity and cost involved with such experiments. Therefore, the development of engineered PINCs from high energetic electrical arcs is highly desirable. PMMA is an ideal base polymer matrix due to its light weight, high impact resistance and lower molecular activation energy [27,30–33] in addition to the proved experimental tests with the arcs [19,34,35]. Among the inorganic nanoparticles, ZnO nanoparticles are classified as strong UV absorbing materials, playing a key role for giving protection from UV radiation from the sun in several health care products like sunscreen and lip care liquids [36–39]. Their high band gap energy of 3.3 eV and their well-developed, chemical synthesis process increase their attractivity [40–42]. When the size of ZnO nanoparticles is close to ~4 nm nm they show photoluminescence by absorbing broad range UV radiation, caused to recombination of the acceptor-bound excitons at room temperature. In this size regime these nanoparticles are named as QDs due to demonstration of quantum size effects [43,44].

The aim of this work is to develop efficient PINCs in order to cool down and quench the electrical arcs by effectively absorbing the intense UV radiation emitted from the electrical arcs generated in the circuit breaker. Such PINCs should be able to withdraw more energy from the electrical arcs in comparison to ordinary polymers for improving the arc interruption capability of electrical switching applications. This paper is the first of its kind on the electrical arcs

influenced by the ZnO QDs based PINCs, which are specifically designed for improving the broad range UV radiation absorption. The synthesis of ZnO QDs as well as their embedment into PMMA matrix by *in-situ* sol-gel polymerization [17,19] to fabricate PINCs has been described in detail. Besides that, the impact of such PINCs on the electrical properties of electrical arcs (i.e. operational limits) generated by using the synthetic RLC circuit [9,45] and designed test-setup at KTH laboratory is demonstrated. These measurements are aimed at improving our understanding on the arc interruption capability via a careful study of total dissipated energy versus the ablation rates and the arc interruption times during the tests with PINCs.

## 2. Experimental section

### 2.1. Synthesis of ZnO QDs

ZnO QDs were synthesized by hydrolyzing zinc acetate dihydrate ( $\text{Zn}(\text{CH}_3\text{COO})_2 \cdot 2\text{H}_2\text{O}$ , ZAD, > 98% ACS reagent, Sigma-Aldrich) with Ethanolamine –or monoethanolamine (MEA, ≥99% Reagent-Plus®, Sigma-Aldrich) as described by Znaidi et al. [40]. The typical synthesis process was as follows: Zn(II) solution (0.01–0.1 M) was prepared by refluxing ZAD in ethanol (Solveco) at 85 °C for two hours under continuous stirring. Then, MEA was added w.r.to the ratio i.e.  $[\text{MEA}]/[\text{Zn(II)}] = 3$  to these solutions to obtain a desired size of ZnO QDs. The resulting suspension can be varied from transparent to colored (bluish to yellow) depending on the respective concentrations of  $[\text{Zn(II)}]$  and  $[\text{MEA}]$ .

### 2.2. Fabrication of PINCs

Six PINCs were fabricated with different weight percentages (wt %) of synthesized ZnO QDs in methyl methacrylate (MMA) monomer (99%, Sigma-Aldrich) by *in-situ* polymerization [17] and [19]. Specifically, from same suspension of ZnO QDs, different volumes were added to the glass molds containing MMA monomer (5 mL) separately resulting different wt % of ZnO as detailed in Table 1. To initiate polymerization, recrystallized 2,2'-Azobis (2-methylpropionitrile) (AIBN, 98%, Sigma-Aldrich) was added as an initiator to the monomer solutions and dispersed by sonication. Then, the polymerization in the glass molds was carried out at 75 °C for 10 h in a temperature controlled oil bath under mechanical stirring. Polymerization process was completed after ethanol was evaporated and then transparent PINCs were obtained.

### 2.3. Experimental test set-up

The experimental set-up was described earlier by Doddapaneni et al. [19,45] which is comprised of: 1) the synthetic RLC circuit as a current source; and 2) test-setup for discharging the current in between the two hemi spherical contacts. The synthetic RLC circuit consists of a capacitor (16 mF), an inductor (496 μH) for creating a damped oscillation at a frequency of 50 Hz. A thyristor switch was connected in series for switching the current. The capacitor was charged to 450 V for all the discharges in order to generate reproducible electrical arcs with an equivalent peak current of 1.6 kA, approximately. The test-setup (as shown in Fig. 1) was connected in

Table 1  
Content (in wt %) of ZnO QDs in PMMA used for investigated PINCs.

Sample name	PINC_1	PINC_2	PINC_3	PINC_4	PINC_5	PINC_6
ZnO QDs (wt %)	0.01	0.025	0.05	0.075	0.1	0.25

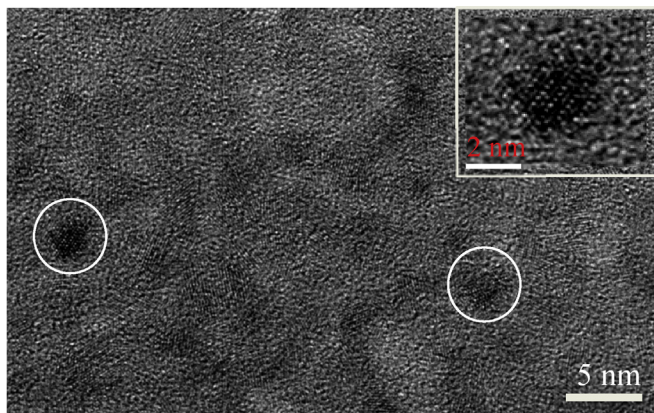


Fig. 2. High resolution TEM image of the ZnO@MEA QDs. Inset enlarged image of a single crystalline ZnO QD.

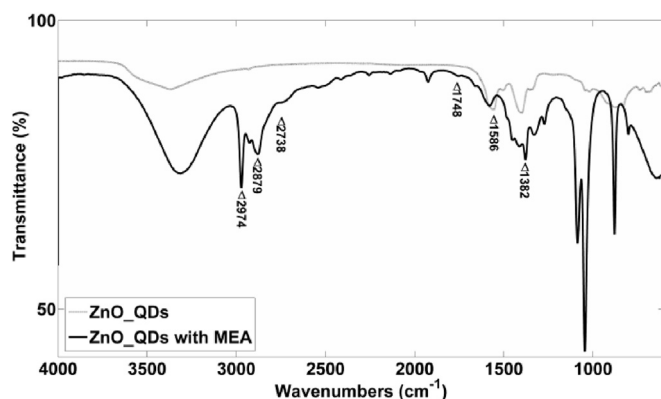


Fig. 3. FTIR spectrum of ZnO QDs with and without MEA.

parallel to the discharged circuit and the electric arcs were generated between the two semi spherically shaped contacts (electrodes) separated by a distance of 5 mm. A thin copper wire of diameter of 20  $\mu\text{m}$  was used for igniting the electrical arc. PINCs and non-ablating quartz slide were placed next to the electrodes in this test-setup in order to observe the impact of PINCs on the electrical arcs and arc interruption capability by the PINCs.

#### 2.4. Characterization methods

Morphology of the synthesized nanoparticles was observed by using transmission electron microscopy (TEM, JEOL 2100) at an acceleration voltage of 200 kV. Fourier transform infrared spectroscopy (FTIR) analyses of solid and liquid samples were examined with Thermo Scientific IR spectrometer (Avatar 360 E.S.P., Nicolet). Inductively coupled plasma optical emission spectrometry (ICP-OES, iCAP 6500, Thermo SCIENTIFIC) was used to measure the concentration of ZnO QDs. The electrical signals, i.e., arc

current and voltage generated on the PINCs and PMMA were recorded by using oscilloscope Picoscope 4824. Mass loss of the PINCs was weighed during the testing on a digital analytical balance with 0.1 mg readability. Surface morphology of the ablated PINCs after experimental testing was studied by using scanning electron microscopy (SEM, Zeiss Ultra 55) and high-resolution optical microscopy (Nikon M13). The UV radiation absorption was evaluated by using UV–Vis spectrometer (Cary 100 Bio, Varian).

### 3. Results and discussion

As-prepared ZnO QDs have been studied by TEM before *in-situ* polymerization. The TEM micrograph presented in Fig. 2 reveals that the QDs are nearly spherical with particle diameter of  $3.5 \pm 0.6$  nm (estimated by counting > 200 QDs on several micrographs). In addition to that, two theoretical models are used to estimate particle diameter of ZnO QDs; namely effective mass model (EMM) [46,47], and Meulenkamp equation (ME) [37]. The details of the models are presented in the supplementary file. The particle diameter estimated are  $3.1 \pm 0.5$  nm and  $2.9 \pm 0.4$  nm respectively for EMM and ME, agreeing well with the size obtained from the TEM results.

In the sol-gel synthesis of ZnO QDs, MEA aids in hydrolyzing ZAD as well as coupling between QDs and PMMA matrix. In general, MEA extends into the nanoparticles surface to lose their conformational entropy and to inhibit the particle agglomeration in polymer matrix by steric repulsion [40]. In the fabrication of the PINCs, QDs are simultaneously synthesized while MMA monomer polymerizes via free-radical polymerization, which facilitates covalent bonding between ZnO QDs and PMMA matrix.

Plain ZnO QDs and QDs with MEA coating are analyzed using FTIR spectroscopy; the spectra are shown in Fig. 3. The plain QDs show a broad absorption peak at  $3250\text{--}3850$   $\text{cm}^{-1}$ , which can be assigned to  $\text{--OH}$  stretching. The peaks at  $1586$ ,  $620$   $\text{cm}^{-1}$  are correspond to  $\text{Zn--O}$  stretching and deformation vibration, respectively. In the spectrum for coated ZnO QDs  $\text{--NH}$  peak is observed at  $3300$   $\text{cm}^{-1}$ , showing the presence of MEA, which is used for hydrolyzing the ZAD. The surface of MEA coated QDs is anchored with  $\text{--CH}$ ,  $\text{--CH}_2$  and  $\text{--CH}_3$  stretching  $2750\text{--}3000$ ,  $1382$   $\text{cm}^{-1}$ , and  $\text{C=O}$  stretching ( $1748$   $\text{cm}^{-1}$ ) are observed in the FTIR spectrum [19,35].  $\text{C=O}$  stretching evidenced carbonyl group on QDs surface due to oxidation of MEA or residual acetate from ZAD. MEA helps to avoid agglomeration among the ZnO QDs during the polymerizations process.

Six PINCs of thickness 0.5 cm and diameter 2.5 cm are fabricated by using *in-situ* sol-gel polymerization process [17]. while pure PMMA is also fabricated by the identical polymerization process, but without QDs as displayed in Fig. 4. There are six PINCs and PMMA, named as PINC\_1, PINC\_2, PINC\_3, PINC\_4, PINC\_5 and PINC\_6 based on wt % of the ZnO QDs suspension as listed in Table 1. The aim of these PINCs is to evaluate the threshold wt % of ZnO QDs in PMMA matrix where it leads to the best arc interruption capability. In addition, it helps to

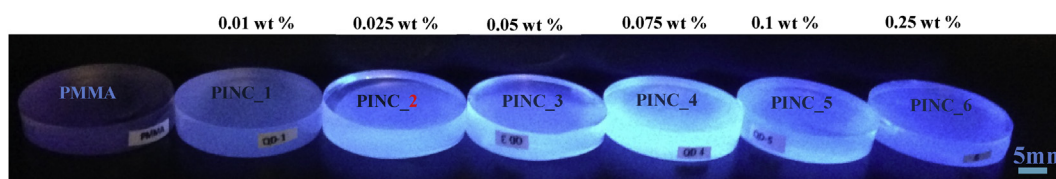


Fig. 4. Photograph of the fabricated PMMA and the PINCs under low intensity UV lamp with different wt % of ZnO QDs.

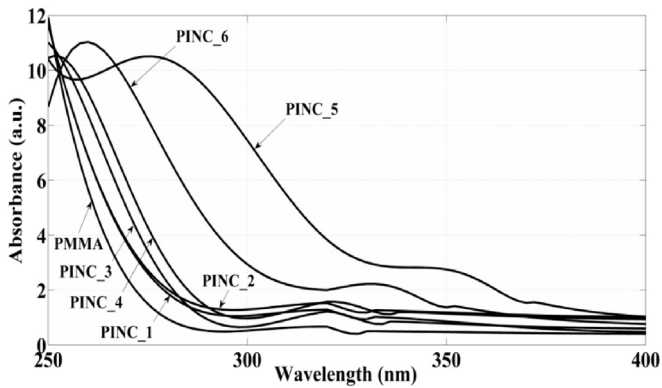


Fig. 5. UV–vis absorption spectra of all the PINCs and PMMA.

understand the impact of broad range radiation absorption from the electrical arcs. In general, the PINCs have an issue of homogeneity due to nanoparticles size dispersion, agglomeration, and interaction with the polymer matrix. In this work MEA is used effectively for improving the miscibility and dispersibility of ZnO QDs within PMMA matrix via in situ sol-gel polymerization process [17]. Fig. 4 depicts a photograph of bulk transparent PINCs containing different wt % of ZnO QDs under a low intensity UV light ( $\lambda = 362$  nm) irradiation. The fluorescence emission increases with increasing wt % of ZnO QDs and then starts to decay, which might be due to percolation threshold and short-range interactions between the QDs that cause quenching. Xiong et al. reported a similar observation [48], where they have utilized ZnO fillers for fabricating poly (styrene butylacrylate) latex-ZnO nanocomposites. Based on fluorescence emissions displayed in Fig. 4, PINCs containing the different wt % of ZnO QDs used in this work exhibits homogeneous distribution. It could be due to fine dispersion of ZnO QDs with a larger free space between them in addition to superior interfacial link between the attained heterogeneous phases. UV–Vis analysis of the PMMA and PINCs demonstrated that the absorption edge systematically and stepwise increases from PMMA till PINC\_5, while decreased for PINC\_6 as shown in Fig. 5. It is noticed that the UV absorption edges of PMMA and all the PINCs are in order of 270 nm, 278 nm, 279 nm, 284 nm, 288 nm, 338 nm and 306 nm

respectively as also listed in Table 2. It is also observed that the inversion in the absorption edge for PINC\_6 due to the increased wt % of QDs over percolation threshold level in PMMA matrix. It is not much surprising due to the fact that the UV absorption spectra followed the trend of fluorescence intensity of the samples.

The electrical arcs (of current  $\sim 1.6$  kA) are produced between two hemispherical shaped electrodes in the designed test-setup (Fig. 1), used for testing the arc interruption capability of the fabricated PINCs [35,45]. All the fabricated PINCs shown in Fig. 4 are tested on front and backside in order to test reproducibility of arc interruption capability. New copper contacts and fresh quartz slides are used for all the tests. The recorded arc voltage and current signals are shown in Fig. 6. While testing the PINCs and PMMA, all the samples were weighed before and after testing using a microbalance in order to obtain the ablated mass values. Ablation rates coupled with the total dissipated energy i.e.,  $\int I(t)V(t)dt$  from the electrical signals are shown in Fig. 7. Ablation rates are calculated by the ratio of experimentally obtained ablated masses and computed dissipated energies [13,49], and are listed in Table 3.

Even though the electrical arc interruption process is statistical in its nature, the following conclusions can be deduced from the measurement results shown in Fig. 6. According to the electrical signals, the ignition wire is evaporated at 1 ms and an electrical arc is generated as shown clearly in the supplementary video file (filename: test with PINC\_4 frontside). The voltage and current signals from Fig. 6 clearly depict the two states of the electrical arc i.e. high-voltage (HV) and low-voltage (LV) state. In HV state, the voltage starts to build-up with the electrical arc due to the presence of ablated chemical species. The addition of ablated chemical species to the arc core causes a drop in the temperature leading to a reduction of the electrical conductivity and an increase of the arc voltage. Interestingly, the voltage build-up is increasing with the wt % of QDs but undergoes a sudden transition from a HV state for lower wt % to a LV state for higher wt %. A similar behavior was observed in our previous studies using iron oxide based nanocomposites [27]. The arc interruption time is a measure for the current interruption capability of the arc. A HV state results in a fast current limitation and an early current interruption, in contrast to LV state. The arc interruption times are extracted from the electrical signals and are listed in Table 3 for all test samples. In case of

Table 2

Observed optical radiation absorption edges (nm) in UV–Vis absorption spectrum (in Fig. 5) of the PMMA, and PINCs.

Sample name	PMMA	PINC_1	PINC_2	PINC_3	PINC_4	PINC_5	PINC_6
Absorption edge $\lambda$ (nm)	270	278	279	284	288	338	306

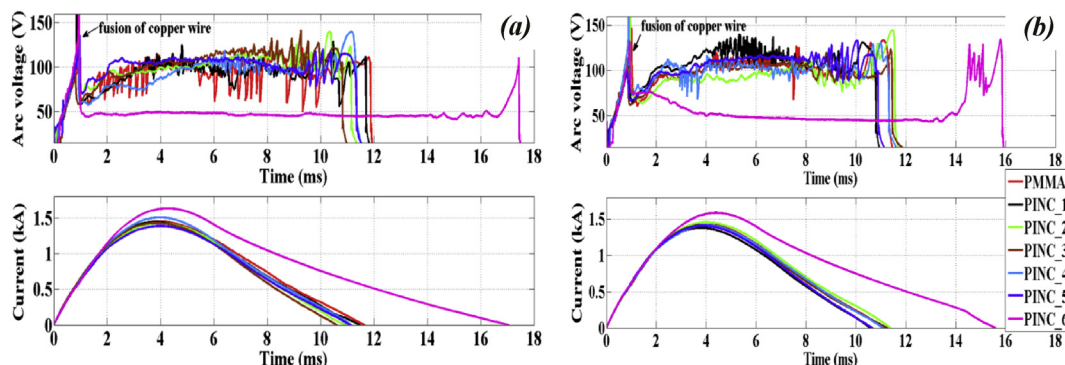


Fig. 6. The electrical signals i.e. Arc voltage and current of the samples frontside (a) and backside (b).

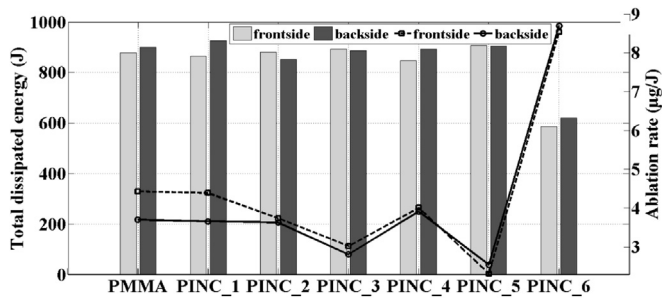


Fig. 7. Impact of ZnO QD wt % on the both sides of PINCs, the total dissipated energy of the electrical arc (bar plot) and ablation rate (solid and dashed lines).

frontside tests, PINCs from PINC\_1 to PINC\_5 exhibited shorter arc interruption times compared to PMMA and lead to electrical arcs that are more stable and produce less back-ignition, which is visible in the reduced number of voltage spikes in the voltage signals. It is worth to mention that PINCs showed a homogeneous dispersion of different wt % of QDs and stepwise increase in UV radiation absorption, which might be responsible for the improvement of the flow of ablated chemical species in a controlled manner towards the electrical arc [49,50]. In case of PINC\_6, the increase in the content of QDs from 0.1 to 0.25 wt % causes an abrupt change in the electric signal and an arc in the low voltage state is produced. In this state, the arc interrupts smoothly without any visible back-ignitions in both at the frontside and the backside tests. Furthermore, it is interesting to note that while for lower wt % of QDs in PMMA matrix increases the UV radiation absorption and the HV state is found, a further increase in wt % of QDs leads to a reduction of UV radiation absorption and state of the arc changes into the LV state.

Supplementary video related to this article can be found at <http://dx.doi.org/10.1016/j.compscitech.2017.01.017>.

Total dissipated energy coupled to the ablation rate, shown in Fig. 7, help to understand the arc interruption capability of the PINCs and PMMA. According to the dissipated energy and ablation rates, pure PMMA ablates a lower amount of chemical species towards the electrical arc, revealing a number of fast varying voltage spikes [35,49] and a smooth surface morphology. In case of frontside and backside tests, PINCs up to PINC\_5 showed better arc interruption capability by causing a higher amount of dissipated energy. Nevertheless, the measured ablation rate of PINCs is low and a non-monotonous variation of the ablated mass values while increasing wt % of QDs is found, as shown in Table 3. The reduction of ablated mass for the samples up to PINC\_5 could possibly be explained by either an increase of the re-deposition of polymeric fragments and soot on the PINCs surfaces, or by a shielding of the polymer bulk from UV radiation. In the latter case, the UV radiation would only affect the polymer surface and lead to a more controlled ablation of chemical species, while reducing the amount of larger fragments. In summary, the increase of wt % up to 0.1 leads to an increase of UV radiation absorption and a reduction of the ablated mass, leading to an electrical arc in the HV state. Between of 0.1 and 0.25 wt % the electrical arc undergoes a sudden transition into the

LV state while the UV radiation absorption is also reduced and the amount of ablated mass is increased.

Surface morphology of the PMMA and PINCs has been evaluated by SEM after exposure to the electrical arcs in the test set-up; few micrographs are shown in Fig. 8. A higher erosion density is visible on the PINCs surface at the anode side and less towards cathode side, due to the fact that high energetic electrons initiate from cathode to anode under extreme conditions. It is almost flat on the PINCs surface close to the center of the electrodes due to the surface re-modifications caused by highly intense radiative and thermal energy interactions [35,45]. The erosion looks like small holes and is more uniform in PINC\_1, PINC\_2, which could be due to largely separated nanoparticles with lower wt %. It is clearly observed that the traces of exploded blisters on the cathode side of PINC\_3, PINC\_4 and PINC\_5 could be due to homogeneous distribution of increased wt % of QDs compared to polymer and nevertheless, improved UV radiation absorption. It is also observed that the trend of the erosion density on the surface of PINCs is in agreement with radiation absorption shift shown in UV–vis spectrum. Such strong erosion intensity on the PINCs could be due to ablation enthalpy of nanoparticles cause the local hot spots via absorption of broad range UV radiation, and causes local high temperatures leading to strong ablation features.

#### 4. Conclusion

A series of bulk homogeneous and transparent PINCs are successfully fabricated with low wt % ZnO QDs loadings by using an *in-situ* nanoparticle synthesis process simultaneously with the polymerization process. Thus six homogeneous samples with various loading of ZnO QDs from 0.01 to 0.25 wt % in PMMA matrix have been fabricated. These PINCs have been characterized in detail for the morphology of QDs, interaction between ZnO QDs and polymer matrix, and ultraviolet (UV) radiation absorption. ZnO QDs have been assessed to have particle diameter of 3.5 nm, by using two theoretical models and their presence in the PMMA is revealed improved UV radiation absorption. UV radiation absorption analysis of the PMMA and PINCs revealed that the absorption edge of PMMA increased stepwise from 278 to 330 nm with increasing wt % of ZnO QDs.

The electric arc interruption capability, electrical signals, ablation rate and arc interruption time of the PINCs are investigated using the designed test set-up. The electrical signals depict the two states of the electrical arc i.e. high voltage and low voltage state. As increasing the wt % of QDs in the PMMA matrix to  $\geq 0.1$  wt %, the electrical arc undergoes a sudden transition from a high voltage to a low voltage state. It is due to the amount of ablated mass varies with the wt % in a non-monotonous way and is correlated to the UV absorption edge. The PINCs do not vary significantly in terms of the total dissipated energy and ablation rate for all the tests. Electron microscope images on the ablated PINCs show the variation in blister size and erosion density w.r.to ZnO QDs wt % in the PMMA matrix.

Our experimental findings from the electrical signals show superior arc interruption capability by using PINCs, and they are reliable and reproducible. The reported results showed that these

Table 3

Computed data using the experimental tests with both sides of the PMMA, PINCs.

Sample name		PMMA	PINC_1	PINC_2	PINC_3	PINC_4	PINC_5	PINC_6
Frontside	Ablation rate ( $\mu\text{g}/\text{J}$ )	4.43	4.39	3.74	3.02	4.01	2.31	8.53
	Arc interruption time (ms)	12.03	11.85	11.31	10.98	11.49	11.5	17.47
Backside	Ablation rate ( $\mu\text{g}/\text{J}$ )	3.7	3.66	3.63	2.81	3.91	2.54	8.70
	Arc interruption time (ms)	11.44	10.92	11.69	11.58	11.43	11	15.91

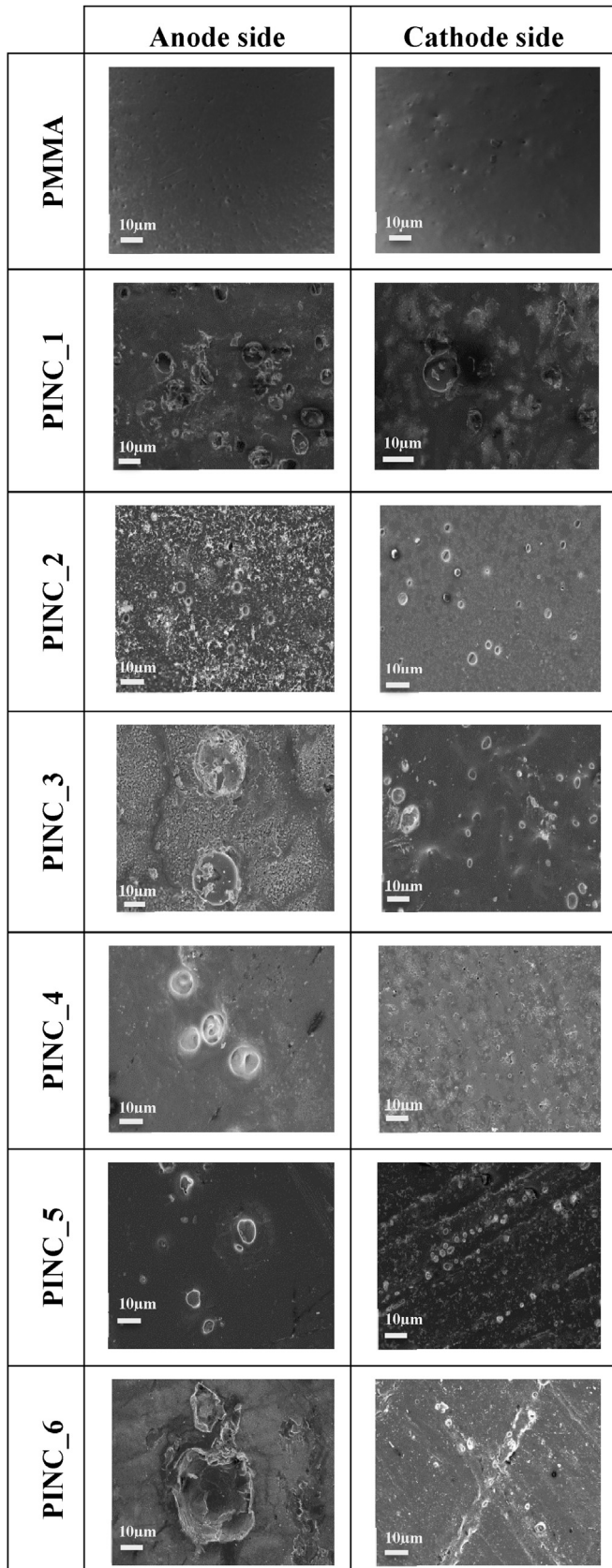


**Fig. 8.** SEM micrographs of all the PINCs on the frontside after three discharges. PINCs are at the anode side (left-side) and cathode side (right-side).

PINCs are promising materials to replace the traditional polymers in the electrical switching applications like circuit breakers.

#### Acknowledgement

This project is partially supported by the Swedish Research Council (VR) under Nanohex project (D0564701), and Swedish Foundation for Strategic Research (SSF, Grant no EM11-0002). VD is thankful to Prof. Hans Edin and Prof. Rajeev Thottappillil, Department of the electromagnetic engineering at KTH for the technical discussions and financial support during these studies. VD would like to thank Dr. Ara Bissal and Mr. Jesper Magnusson, ABB Corporate Research, Sweden for their assistance during the experiments with test-setup.

#### Appendix A. Supplementary data

Supplementary data related to this article can be found at <http://dx.doi.org/10.1016/j.compscitech.2017.01.017>.

#### References

- [1] R.D. Van Buskirk, C.L.S. Kantner, B.F. Gerke, S. Chu, A retrospective investigation of energy efficiency standards: policies may have accelerated long term declines in appliance costs, *Environ. Res. Lett.* 9 (11) (2014) 114010–114021.
- [2] A. Savaresi, The Paris Agreement: a new beginning? *J. Energy Nat. Resour. Law* 34 (1) (2016) 16–26.
- [3] M.M. González, O.C. Calero, P.D. Chao, Nanoengineering thermoelectrics for 21st century: energy harvesting and other trends in the field, *Renew. Sustain. Energy Rev.* 24 (2013) 288–305.
- [4] C. Gao, G. Chen, Conducting polymer/carbon particle thermoelectric composites: emerging green energy materials, *Compos. Sci. Technol.* 124 (2016) 52–70.
- [5] M. Seeger, Perspectives on research on high voltage gas circuit breakers, *Plasma Chem. Plasma Process.* 35 (3) (2015) 527–541.
- [6] D. Eichhoff, A. Kurz, R. Kozakov, G. Gott, D. Uhrlandt, A. Schnettler, Study of an ablation-dominated arc in a model circuit breaker, *J. Phys. D Appl. Phys.* 45 (30) (2012) 305204–305214.
- [7] Y. Cressault, J.M. Bauchire, D. Hong, H. Rabat, G. Riquel, F. Sanchez, A. Gleizes, Radiation of long and high power arcs, *J. Phys. D Appl. Phys.* 48 (41) (2015) 415201–415214.
- [8] J. Sun, B. Zhang, H.E. Katz, Materials for printable, transparent, and low-voltage transistors, *Adv. Funct. Mater.* 21 (1) (2011) 29–45.
- [9] E. Jonsson, M. Runde, G. Dominguez, A. Friberg, E. Johansson, Comparative study of arc-quenching capabilities of different ablation materials, *IEEE Trans. Power Deliv.* 28 (4) (2013) 2065–2070.
- [10] C.M. Dixon, J.D. Yan, M.T.C. Fang, A comparison of three radiation models for the calculation of nozzle arcs, *J. Phys. D Appl. Phys.* 37 (23) (2004) 3309–3318.
- [11] R. Frank, G. Jean-Jacques, F. Pierre, Modelling and simulation of radiative energy transfer in high-voltage circuit breakers, *J. Phys. D Appl. Phys.* 45 (37) (2012) 375201.
- [12] L. Niemeyer, Evaporation dominated high current arcs in narrow channels, *IEEE Trans. Power Appar. Syst.* PAS 97 (3) (1978) 950–958.
- [13] C.B. Ruchti, L. Niemeyer, Ablation controlled arcs, *IEEE Trans. Plasma Sci.* 14 (4) (1986) 423–434.
- [14] Y. Tanaka, Y. Takeuchi, T. Sakuyama, Y. Uesugi, S. Kaneko, S. Okabe, Numerical and experimental investigations on thermal interaction between thermal plasma and solid polymer powders using induction thermal plasma technique, *J. Phys. D Appl. Phys.* 41 (2) (2008) 025203–025218.
- [15] V.V. Nossov, B. Hage, B. Jusselin, C. Fiévet, Simulation of the thermal radiation effect of an arc on polymer walls in low-voltage circuit breakers, *Tech. Phys.* 52 (5) (2007) 651–659.
- [16] S. Ramakrishnan, A.D. Stokes, J.J. Lowke, An approximate model for high-current free-burning arcs, *J. Phys. D Appl. Phys.* 11 (16) (1978) 2267–2280.
- [17] S. Li, M. Meng Lin, M.S. Toprak, D.K. Kim, M. Muhammed, Nanocomposites of polymer and inorganic nanoparticles for optical and magnetic applications, *Nano Rev.* 1 (0) (2010) 1–19.
- [18] P.F. Hettwer, Arc-interruption and gas-evolution characteristics of common polymeric materials, *IEEE Trans. Power Appar. Syst.* 101 (6) (1982) 1689–1696.
- [19] V. Doddapaneni, Y.C. Zhao, F. Ye, R. Gati, H. Edin, M.S. Toprak, Improving UV radiation absorption by copper oxide NPs/PMMA nanocomposites for electrical switching applications, *Powder Metall. Metal Ceram.* 54 (7–8) (2015) 397–401.
- [20] J. Gu, C. Liang, J. Dang, W. Dong, Q. Zhang, Ideal dielectric thermally conductive bismaleimide nanocomposites filled with polyhedral oligomeric silsesquioxane functionalized nanosized boron nitride, *RSC Adv.* 6 (42) (2016) 35809–35814.

- [21] J. Gu, N. Li, L. Tian, Z. Lv, Q. Zhang, High thermal conductivity graphite nanoplatelet/UHMWPE nanocomposites, *RSC Adv.* 5 (46) (2015) 36334–36339.
- [22] J. Gu, X. Yang, Z. Lv, N. Li, C. Liang, Q. Zhang, Functionalized graphite nanoplatelets/epoxy resin nanocomposites with high thermal conductivity, *Int. J. Heat Mass Transf.* 92 (2016) 15–22.
- [23] H. Zhang, J. Han, B. Yang, Structural fabrication and functional modulation of nanoparticle–polymer composites, *Adv. Funct. Mater.* 20 (10) (2010) 1533–1550.
- [24] Y. Zhang, F. Wang, E. Ju, Z. Liu, Z. Chen, J. Ren, X. Qu, Metal-organic-framework-based vaccine platforms for enhanced systemic immune and memory response, *Adv. Funct. Mater.* 26 (35) (2016) 6454–6461.
- [25] Y. Yang, J. Ouyang, L. Ma, R.J.H. Tseng, C.W. Chu, Electrical switching and bistability in organic/polymeric thin films and memory devices, *Adv. Funct. Mater.* 16 (8) (2006) 1001–1014.
- [26] J. Gu, X. Yang, C. Li, K. Kou, Synthesis of cyanate ester microcapsules via solvent evaporation technique and its application in epoxy resins as a healing agent, *Ind. Eng. Chem. Res.* 55 (41) (2016) 10941–10946.
- [27] S. Wei, J. Sampathi, Z. Guo, N. Anumandla, D. Rutman, A. Kucknoor, L. James, A. Wang, Nanoporous poly(methyl methacrylate)-quantum dots nanocomposite fibers toward biomedical applications, *Polymer* 52 (25) (2011) 5817–5829.
- [28] G.A. Sotiriou, C.O. Blattmann, S.E. Pratsinis, Flexible, multifunctional, magnetically actuated nanocomposite films, *Adv. Funct. Mater.* 23 (1) (2013) 34–41.
- [29] S. Parola, B.J. López, L.D. Carlos, C. Sanchez, Optical properties of hybrid organic-inorganic materials and their applications, *Adv. Funct. Mater.* 26 (36) (2016) 6506–6544.
- [30] H. Zweifel, *Stabilization of Polymeric Materials*, Springer-Verlag, Berlin, 1997.
- [31] H. Zweifel, R. Maier, M. Schiller, *Plastics Additives Handbook*, 6 ed., Hanser-Verlag, München, 2009.
- [32] J. Jang, J.H. Oh, Fabrication of a highly transparent conductive thin film from polypyrrole/poly(methyl methacrylate) core/shell nanospheres, *Adv. Funct. Mater.* 15 (3) (2005) 494–502.
- [33] Z. Guo, L.L. Henry, V. Palshin, E.J. Podlaha, Synthesis of poly(methyl methacrylate) stabilized colloidal zero-valence metallic nanoparticles, *J. Mater. Chem.* 16 (18) (2006) 1772–1777.
- [34] Y.L. Hsin, C.F. Lin, Y.C. Liang, K.C. Hwang, J.C. Horng, J.A. Ho, C.C. Lin, J.R. Hwu, Microwave arcing induced formation and growth mechanisms of core/shell metal/carbon nanoparticles in organic solutions, *Adv. Funct. Mater.* 18 (14) (2008) 2048–2056.
- [35] V. Doddapaneni, S. Mohsin, F. Ye, R. Gati, M.S. Toprak, On the electric arc interruption in air by using iron oxide and PMMA nanocomposites, *Mater. Res. Express* 3 (10) (2016) 105043–105051.
- [36] W.J. Beek, M.M. Wienk, M. Kemerink, X. Yang, R.A. Janssen, Hybrid zinc oxide conjugated polymer bulk heterojunction solar cells, *J. Phys. Chem. B* 109 (19) (2005) 9505–9516.
- [37] E.A. Meulenkaamp, Synthesis and growth of ZnO nanoparticles, *J. Phys. Chem. B* 102 (29) (1998) 5566–5572.
- [38] G. Bai, M.K. Tsang, J. Hao, Luminescent ions in advanced composite materials for multifunctional applications, *Adv. Funct. Mater.* 26 (35) (2016) 6330–6350.
- [39] Z. Guo, S. Wei, B. Shedd, R. Scaffaro, T. Pereira, H.T. Hahn, Particle surface engineering effect on the mechanical, optical and photoluminescent properties of ZnO/vinyl-ester resin nanocomposites, *J. Mater. Chem.* 17 (8) (2007) 806–813.
- [40] L. Znaidi, G.J.A.S. Illia, S. Benyahia, C. Sanchez, A.V. Kanaev, Oriented ZnO thin films synthesis by sol-gel process for laser application, *Thin Solid Films* 428 (1–2) (2003) 257–262.
- [41] R.S. Devan, R.A. Patil, J.H. Lin, Y.R. Ma, One-dimensional metal-oxide nanostructures: recent developments in synthesis, characterization, and applications, *Adv. Funct. Mater.* 22 (16) (2012) 3326–3370.
- [42] Y.H. Kim, J.S. Kim, W.M. Kim, T.Y. Seong, J. Lee, L. Müller-Meskamp, K. Leo, Realizing the potential of ZnO with alternative non-metallic co-dopants as electrode materials for small molecule optoelectronic devices, *Adv. Funct. Mater.* 23 (29) (2013) 3645–3652.
- [43] K.P. Musselman, S. Albert-Seifried, R.L.Z. Hoyer, A. Sadhanala, D. Muñoz-Rojas, J.L. MacManus-Driscoll, R.H. Friend, Improved exciton dissociation at semiconducting polymer:ZnO donor:acceptor interfaces via nitrogen doping of ZnO, *Adv. Funct. Mater.* 24 (23) (2014) 3562–3570.
- [44] O. Lupan, T. Pauporté, T. Le Bahers, B. Viana, I. Ciofini, Wavelength-emission tuning of ZnO nanowire-based light-emitting diodes by Cu doping: experimental and computational insights, *Adv. Funct. Mater.* 21 (18) (2011) 3564–3572.
- [45] V. Doddapaneni, J. Magnusson, A. Bissal, H. Edin, M.S. Toprak, R. Gati, Spectroscopic investigations of the ablated species from the polymers exposed to electric arcs in air, in: 2015 3rd International Conference on Electric Power Equipment - Switching Technology (ICEPE-ST), vol. 3, 2015, pp. 337–340.
- [46] L.E. Brus, Electron–electron and electron-hole interactions in small semiconductor crystallites: the size dependence of the lowest excited electronic state, *J. Chem. Phys.* 80 (9) (1984) 4403–4409.
- [47] L. Brus, Electronic wave functions in semiconductor clusters: experiment and theory, *J. Phys. Chem.* 90 (12) (1986) 2555–2560.
- [48] M. Xiong, G. Gu, B. You, L. Wu, Preparation and characterization of poly(styrene butylacrylate) latex/nano-ZnO nanocomposites, *J. Appl. Polym. Sci.* 90 (7) (2003) 1923–1931.
- [49] E. Doméjean, P. Chévrier, C. Fiévet, P. Petit, Arc-wall interaction modelling in a low-voltage circuit breaker, *J. Phys. D Appl. Phys.* 30 (15) (1997) 2132–2142.
- [50] F. Yang, Y. Wu, M.Z. Rong, H. Sun, A.B. Murphy, Z.G. Ren, C.P. Niu, Low-voltage circuit breaker arcs-simulation and measurements, *J. Phys. D Appl. Phys.* 46 (27) (2013) 273001–273019.